Progress In Electromagnetics Research B, Vol. 23, 165–180, 2010

THEORETICAL ANALYSIS OF A PASSIVE ACOUSTIC BRAIN MONITORING SYSTEM

N. P. Asimakis, I. S. Karanasiou, P. K. Gkonis and N. K. Uzunoglu

Microwave and Fiber Optics Laboratory
School of Electrical and Computer Engineering
National Technical University of Athens
9, Iroon Polytechneiou Street, 157 80, Zografou Campus
Athens, Greece

Abstract—An approach based on acoustics and its theoretical analogies to electromagnetism is used in the present research to study the detection of the acoustic wave energy radiated by the thermal random motion of material particles of the brain during activation or caused by pathology. Pressure and particle velocity are calculated in analytical mathematical forms for the case of human brain monitoring, which can be implemented by a prototype passive acoustic brain monitoring system (PABMOS). A sphere to model the human head and an internal point source in order to simulate potential pressure alterations due to intracranial abnormalities or local functional activations, are used in the theoretical representation of the present approach. Finally, numerical results for arbitrary positions of the internal source, concerning the particle velocity (pressure field distribution) at the surface of the head model which can implicitly be measured by the suitable piezoelectric sensors, are presented.

1. INTRODUCTION

The propagation of sound is always associated with the medium; sound, contrary to electromagnetic waves, does not propagate in vacuum. Sound is generated when the medium is dynamically disturbed, causing its particles to vibrate around their mean position and changing their relative displacement and velocity. Such disturbance of the medium propagates in the form of acoustic waves and affects its pressure, density and temperature [1, 2].

Received 31 May 2010, Accepted 13 July 2010, Scheduled 21 July 2010
Corresponding author: N. P. Asimakis (nasimakis@esd.ece.ntua.gr).

In human physiology, arterial conducted heart pulses are coupled to the brain so that the brain pulses in phase with the heart when the time lag for signal propagation is taken into account. However, when the brain functionality is disturbed by injury, disease or is excited by external stimuli, its consistency changes in such way that the signal which is sensed at the skull using a sensitive detecting device does no longer coincides with the arterial pulse wave. This signal arises from functional activation of respective brain regions (volumes) or from phenomena such as lack of perfusion in the brain, edema causing decreased compliance and consequent loss of perfusion, and infarcts which alter the consistency of the brain tissue and hence its acoustic properties. This latter effect characterizes the occurrence of brain tumors as well. Apart from the aforementioned, signal anomalies can also be seen in intra-operative loss of perfusion in the brain where circulation can be impaired for periods of time during procedures such as open-heart surgery. The same principles apply when measuring alterations of flow patterns in the circulatory system arising from impediments to flow, such as clots that may occur downstream from the heart, and can be detected at an artery beyond the clot [3].

Existing clinical systems that are used to assess anomalies such as brain trauma, stroke and tumors, include computed tomography (CT) scans, magnetic resonance imaging (MRI) and, in case of brain trauma monitoring, combinations of these with invasive intra ventricular catheters (IVC) or subarachnoid bolts to directly measure intracranial pressure (ICP). There is, however, currently, no way to determine brain disorder without such equipment, leaving decisions on treatment to be delayed in the case of stroke until it can be determined whether the stroke is a bleed or ischemia. In a similar fashion, persons injured at the scene of an accident must be presumed to be brain injured, even if the cause of their non-responsiveness arises from the effects of drugs or alcohol. Another large category of head injuries are those resulting from falls, particularly in the elderly. Immediate assessment of injury would be most helpful while waiting more comprehensive diagnosis [3].

The non-invasive diagnostic aids that are in use today are continuous wave and pulsed Doppler (Duplex), transcranial Doppler (TCD) and sometimes a combination of magnetic resonance angiography (MRA) and ultrasound which can be useful diagnostic tools for stroke in the hands of a specialist. However, often the accuracy of some of these techniques are technician dependent and are not available to the emergency medical services personnel at the scene where transport decisions must be made [3]. The passive acoustic brain monitoring system could possibly become a solution to all previous immediate, on-scene, head diagnostic needs due to brain injury or

disease.

However, another potential interesting aspect of the proposed system's operation is functional imaging. Functional imaging is currently carried out mainly by functional Magnetic Resonance Imaging (fMRI), Positron Emission Tomography (PET) or Optical Imaging and indirectly based on analysis of data acquired using Electroencephalography (EEG) and Magneto encephalography (MEG),. The aim is to reveal and comprehend how the brain works, in terms of its physiology, functional architecture and dynamics.

At this point it should be noted that recently extensive theoretical and experimental work has been carried out by our research group in using microwave radiometry to develop a prototype imaging system (MiRaIS) [4–7]. The operating principle of the system is based on the use of an ellipsoidal conductive wall cavity for beamforming and focusing on the brain areas of interest. One of the most important advantages of this method is that it operates in an entirely passive and non-invasive manner. MiRaIS has been used for the past 6 years in various experiments in order to evaluate its potential as an intracranial imaging device [4–7]. The MiRaIS system is able to provide real-time temperature and/or conductivity variation measurements in water phantoms and animals and potentially in subcutaneous biological tissues. Importantly, the system has been used in human experiments in order to explore the possibility of passively measuring brain activation changes that are possibly attributed to local conductivity changes. The results indicate the potential value of using focused microwave radiometry to identify brain activations possibly involved or affected in operations induced by particular psychophysiological tasks [5]. If such changes can be detected in the acoustical output signal of the proposed device they could potentially add useful information to the aforementioned well standardized techniques as well as to the information acquired by the MiRaIS. It is obvious from the above-mentioned that a number of biomedical applications regarding monitoring, diagnosis and therapy exists ranging from the acoustic frequency band [8, 9] to microwave techniques (e.g., [10]).

The present paper is mainly focused on the theoretical aspects of the proposed passive acoustic system presenting a configuration of a single layered head model sphere and an internal activation sphere (source) and providing the mathematical formulation for this problem. Additionally, numerical results corresponding to the acoustic energy generated, and detected at the surface of the head model are discussed. The implementation of the prototype acoustic system, that is now tested, is presented along with the respective measurements elsewhere. These measurements are carried out in the range of infrasound to sound

frequencies (1 Hz to approximately 20 kHz) with the use of the suitable piezoelectric sensors and the appropriate phantoms.

2. MATHEMATICAL ANALYSIS OF ACOUSTIC RADIATION INDUCED BY A SOURCE POINT INSIDE A SPHERICAL HEAD MODEL

The theoretical analysis of the present research is based on acoustic theory and its appropriate correspondence to electromagnetism. When a source of acoustic energy is located inside a bounded solid object, acoustic waves are generated causing a pressure field distribution at the surrounding area in the same way that an electric field distribution is obtained by chaotic radiation emitted under the condition of thermodynamic equilibrium of matter with radiation (Max Plank's black body theory). In other words, for acoustic waves, the pressure variation $\bar{p}(\underline{r}, t)$ replaces the electric field $\bar{E}(\underline{r}, t)$ [11]. In order to model the pressure field distribution in the presence of human head, a semi-analytical technique is presented, based on the use of the dyadic's Green's function theory. By imposing the appropriate boundary conditions at a finite number of points on the physical interface of the particular object with air, the unknown coefficients of the dyadic Green's function are determined and therefore the pressure field and the particle velocity is calculated at any arbitrary point of the proposed configuration.

As discussed before, disturbed blood flow affects brain consistency and generates acoustic waves that can be used to investigate its functional characteristics and its abnormal activity. To the direction of configuring this problem, the human head can be modeled with a sphere that has acoustic characteristics (sound velocity and attenuation) related to infrasound and sound frequencies (1 Hz–20 kHz), and variation in blood flow with an internal source. Assuming sphere's radius $r = \alpha$, the source can be placed at a distance r' inside the sphere, oscillating relatively to frequency and creating an internal activation sphere (IAS). The geometry of the problem is depicted in Fig. 1.

The aim of this theoretical analysis is to calculate the emitted acoustic energy in terms of pressure (P) and particle velocity (u) on the surface of the model sphere caused by the internal source, arbitrary located inside the head model. The equations relating these two measures are presented below [12], where ρ is the density of the medium, ρ_0 its equilibrium density, γ the ratio of the heat capacity at constant pressure (C_P) to heat capacity at constant volume (C_V) and

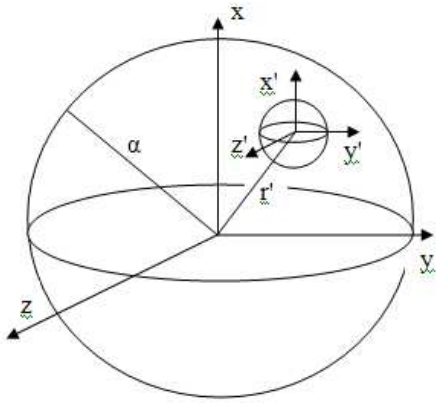

Figure 1. The geometry of the problem.

P_0 the equilibrium pressure:

$$\text{Particle displacement } \vec{\xi}(\underline{r},t) = \nabla P$$

$$\text{Particle velocity } \vec{u}(\underline{r},t) = \frac{\partial \vec{\xi}(\underline{r},t)}{\partial t}$$

$$\text{Condensation } s = -\frac{\partial \vec{\xi}(\underline{r},t)}{\partial x} = \frac{\rho - \rho_0}{\rho_0} = -\nabla \vec{\xi}(\underline{r},t)$$

$$\text{Overpressure } P = \gamma P_0 s = -\gamma P_0 \nabla \vec{\xi}(\underline{r},t)$$

From the relations above and in analogy to electromagnetism the wave equation is derived, regarding the pressure (P) which corresponds to the acoustic waves generated by the internal source. The movement of the medium particles caused by temperature changes is represented by the term $\vec{j}(\underline{r},t)$ in the next wave equation. C is the speed of sound inside a (particular) medium:

$$\nabla^2 P - \frac{1}{c^2}\frac{\partial^2 P(\underline{r},t)}{\partial t^2} = \vec{j}(\underline{r},t) \tag{1}$$

In order to calculate the pressure and eventually the particle velocity produced by the pressure alternations inside the sphere model, at any point of it and therefore at its surface also, Equation (1) has to be solved. Considering the spherical geometry of the problem, the internal source as a point source and P (pressure) as the solution function of Equation (1), the pressure at infinity (free space) and at a distance r from the centre of the sphere is given respectively from the

following known mathematical formulations of Green's function, which are expressed in spherical polar coordinates [13–16]:

$$P_{\omega 0}(\underline{r},\underline{r}') = G_{\omega 0}(\underline{r},\underline{r}') = \frac{e^{-jk|r-r'|}}{4\pi\,|r-r'|} \Leftrightarrow P_{\omega 0}(\underline{r},\underline{r}')$$

$$= G_{\omega 0}(\underline{r},\underline{r}') = ik\sum_{l=0}^{\infty}\sum_{m=-l}^{l} j_l(kr_<)h_l^{(1)}(kr_>)Y_l^m(\theta,\phi)Y^{*m}_l(\theta',\phi') \quad (2a)$$

and

$$P_{\omega}(\underline{r},\underline{r}') = G_{\omega}(\underline{r},\underline{r}') = \sum_{l=0}^{\infty}\sum_{m=-l}^{l} a_{lm}j_l(kr)Y_l^m(\theta,\phi) \quad (2b)$$

where a_{lm} is the unknown coefficient to be determined, $j_l(kr)$ is the spherical Bessel function, $j_l(kr_<)$ is the spherical Bessel function for distances lesser than r, $h_l^{(1)}(kr_>)$ is the spherical first kind Hankel function for distances greater than r and $Y_l^m(\theta,\phi)$ and $Y^{*m}_l(\theta',\phi')$ are the spherical harmonics. The formulas for $Y_l^m(\theta,\phi)$ and k (wave number), are the following:

$$Y_l^m(\theta,\phi) = \sqrt{\frac{2l+1}{4\pi}\frac{(l-m)!}{(l+m)!}}\cdot e^{im\phi}\cdot P_l^m(\cos\theta)$$

and

$$k = \frac{\omega}{c}n$$

where $P_l^m(\cos\theta)$ is the Legendre polynomial and ω the circular frequency.

At the surface of the sphere ($r = \alpha$), the following boundary condition must be satisfied

$$P_{\omega tot}(\underline{r},\underline{r}') = 0 \Rightarrow P_{\omega 0}(\underline{r},\underline{r}') + P_{\omega}(\underline{r},\underline{r}') = 0, \quad (3)$$

which is transformed by Equation (2) to the next:

$$ik\sum_{l=0}^{\infty}\sum_{m=-l}^{l} j_l(kr_<)h_l^{(1)}(kr_>)Y_l^m(\theta,\phi)Y^{*m}_l(\theta',\phi')$$
$$+\sum_{l=0}^{\infty}\sum_{m=-l}^{l} a_{lm}j_l(kr)Y_l^m(\theta,\phi) = 0$$

For $r = \alpha$, we have $r_< \equiv r'$ and $r_> \equiv \alpha$ so the previous relation

becomes:

$$ik\sum_{l=0}^{\infty}\sum_{m=-l}^{l} j_l(kr')h_l^{(1)}(k\alpha)Y_l^m(\theta,\phi)Y^{*m}_{\ l}(\theta',\phi')$$
$$+\sum_{l=0}^{\infty}\sum_{m=-l}^{l} a_{lm}j_l(k\alpha)Y_l^m(\theta,\phi)=0\Rightarrow$$
$$ik\cdot j_l(kr')h_l^{(1)}(k\alpha)Y^{*m}_{\ l}(\theta',\phi')+a_{lm}j_l(k\alpha)=0\Leftrightarrow$$
$$a_{lm}=-ik\frac{j_l(kr')}{j_l(k\alpha)}h_l^{(1)}(k\alpha)Y^{*m}_{\ l}(\theta',\phi') \tag{4}$$

Equation (4) gives the unknown coefficient a_{lm} and together with Equation (2) they can be used to express and calculate the total pressure P_Σ (at the frequency field):

$$G_{\omega tot}(\underline{r},\underline{r}')=P_{\omega tot}(\underline{r},\underline{r}')=P_\omega(\underline{r},\underline{r}')+P_{\omega 0}(\underline{r},\underline{r}')\Leftrightarrow$$
$$G_{\omega tot}(\underline{r},\underline{r}')=ik\sum_{l=0}^{\infty}\sum_{m=-l}^{l} j_l(kr')\left(h_l^{(1)}(kr)-\frac{h_l^{(1)}(k\alpha)}{j_l(k\alpha)}j_l(kr)\right)$$
$$Y_l^m(\theta,\phi)Y^{*m}_{\ l}(\theta',\phi') \tag{5}$$

So far boundary conditions have been used on the sphere's surface and the internal point source was substituted in equations by the impulse function. Considering the internal activation volume (small sphere in Fig. 1) created from the summation of a finite number of point sources (mesh), a new measure is introduced in the basic equations (wave equation, etc.), for the problem in question. This is the volume flow $q(\underline{r},t)$ and is defined as follows:

$$q(\underline{r},t)=\frac{inbound\ volume}{unit\ volume\cdot unit\ time}$$

The new relations that come up regarding pressure and particle velocity are the following:

$$\nabla P(\underline{r},t)=-\rho_0\frac{\partial\vec{u}(\underline{r},t)}{\partial t} \tag{6}$$
$$\nabla\vec{u}(\underline{r},t)=-\frac{1}{\rho_0c^2}\frac{\partial P(\underline{r},t)}{\partial t}+q(\underline{r},t)\Rightarrow$$
$$\nabla^2P(\underline{r},t)-\frac{1}{c^2}\frac{\partial^2P(\underline{r},t)}{\partial t^2}=-\rho_0\frac{\partial q(\underline{r},t)}{\partial t} \tag{7}$$

Calculating the Fourier transform of the new wave Equation (7) for pressure, we have:

$$\nabla^2P_\omega(\underline{r})+\frac{\omega^2}{c^2}P_\omega(\underline{r})=-\rho_0j\omega q_\omega(\underline{r}'),$$

which is the inhomogeneous Helmholtz equation with the next known solution [15, 17]:

$$P_\omega(\underline{r}) = \iiint\limits_V (j\omega\rho_0) G_\omega(\underline{r}, \underline{r'}) q_\omega(\underline{r'}) dr' \Leftrightarrow$$

$$P_\omega(\underline{r}) = j\omega\rho_0 \iiint\limits_V G_\omega(\underline{r}, \underline{r'}) q_\omega(\underline{r'}) dr' \tag{8}$$

where $G_\omega(\underline{r}, \underline{r'})$ is the total dyadic Green's function for the corresponding region, given by relation (5) of the first part of the problem analysis.

As the final part of our brain monitoring system is practically a set of piezoelectric sensors, which substantially measure the particle velocity of a pressure wave, the latter property is consequently calculated in the following analysis. The Fourier transform of Equation (6) is:

$$\nabla P_\omega(\underline{r}) = -\rho_0 (j\omega) \vec{u}^{\omega}(\underline{r}) \Leftrightarrow \vec{u}^{\omega}(\underline{r}) = -\frac{1}{\rho_0 j\omega} \nabla P_\omega(\underline{r})$$

Considering changes in pressure and velocity only at the radial direction r, we finally have:

$$\vec{u}^{\omega}(\underline{r}) = -\frac{1}{\rho_0 j\omega} \frac{\partial}{\partial r} P_\omega(\underline{r}) \overset{(8)}{\Leftrightarrow} u_\omega(\underline{r}) = -\iiint\limits_V \left(\frac{\partial}{\partial r} G_\omega(\underline{r}, \underline{r'}) \right) q_\omega(\underline{r'}) dr'$$

As the particles' velocity cannot be described deterministically (stochastic size), we have to estimate its ensemble average:

$$< u_\omega(\underline{r}) u^*_\omega(\underline{r}) > =$$
$$\iiint\limits_V \left(\frac{\partial}{\partial r} G_\omega(\underline{r}, \underline{r'}) \right) q_\omega(\underline{r'}) dr' \iiint\limits_V \left(\frac{\partial}{\partial r} G^*_\omega(\underline{r}, \underline{r''}) \right) q^*_\omega(\underline{r''}) dr'' \Leftrightarrow$$
$$< u_\omega(\underline{r}) u^*_\omega(\underline{r}) > =$$
$$\frac{1}{\rho_0^2} \iiint\limits_V \left(\frac{\partial}{\partial r} G_\omega(\underline{r}, \underline{r'}) \right) \rho_0 q_\omega(\underline{r'}) dr' \iiint\limits_V \left(\frac{\partial}{\partial r} G^*_\omega(\underline{r}, \underline{r''}) \right) \rho_0 q^*_\omega(\underline{r''}) dr'' \Leftrightarrow$$
$$< u_\omega(\underline{r}) u^*_\omega(\underline{r}) > =$$
$$\frac{1}{\rho_0^2} \iiint\limits_V dr' \iiint\limits_V dr'' \cdot \left(\frac{\partial}{\partial r} G_\omega(\underline{r}, \underline{r'}) \right) \cdot \left(\frac{\partial}{\partial r} G^*_\omega(\underline{r}, \underline{r''}) \right)$$
$$< \rho_0 q_\omega(\underline{r'}) \rho_0 q^*_\omega(\underline{r''}) > \tag{9}$$

In order to calculate the ensemble average $< \rho_0 q_\omega(\underline{r'})\rho_0 q^*_\omega(\underline{r''}) >$ we need to focus on the thermal behavior of the problem, defining the product $\rho_0 q_\omega(\underline{r})$ as follows:

$$\left.\begin{array}{l} \rho_0 q_\omega(\underline{r}) = \dfrac{inbound\ mass}{unit\ volume \cdot unit\ time} \\ \rho_0 q_\omega(\underline{r}) = \frac{\mathrm{N}\cdot(\delta m)\cdot \upsilon_\theta}{l_{eff}} \\ C_{eff} = \frac{N\cdot(\delta m)}{l_{eff}} \quad (10) \end{array}\right\} \rho_0 q_\omega(\underline{r}) = C_{eff} \cdot \upsilon_\theta$$

where N: number of vibrating molecules per unit volume, δm: mass of every molecule, υ_θ: kinetic velocity of particles, l_{eff}: equivalent length of Brownian motion that molecules vibrate. Due to the equations above and as $q_\omega(\underline{r'})$ and $q^*_\omega(\underline{r''})$ are uncorrelated, the wanted average becomes:

$$< \rho_0 q_\omega(\underline{r'})\rho_0 q^*_\omega(\underline{r''}) >=< C^2_{eff}\upsilon_\theta \upsilon^*_\theta >= \delta(\underline{r'} - \underline{r''}) \cdot C^2_{eff} \int\limits_{\upsilon_\theta=0}^{+\infty} \upsilon^2_\theta p(\upsilon_\theta) d\upsilon_\theta$$

It is known that, the Maxwell-Boltzmann distribution for the particle speed is

$$p(\upsilon_\theta) = 4\pi \left(\frac{m}{2\pi kT}\right)^{3/2} e^{-\frac{m\upsilon^2_\theta}{2kT}} \upsilon^2_\theta$$

therefore

$$\begin{aligned} <\rho_0 q_\omega(\underline{r'})\rho_0 q^*_\omega(\underline{r''}) > &= \delta(\underline{r'} - \underline{r''}) \cdot C^2_{eff} \int\limits_{\upsilon_\theta=0}^{+\infty} 4\pi \Big(\frac{m}{2\pi kT}\Big)^{3/2} e^{-\frac{m\upsilon^2_\theta}{2kT}} \upsilon^4_\theta d\upsilon_\theta \\ &= \delta(\underline{r'} - \underline{r''}) \cdot C^2_{eff} \cdot I \end{aligned}$$

Calculating the integral I, we set $a = \frac{m}{2kT}$ and make the variable change $t = \upsilon^2_\theta \Leftrightarrow d\upsilon_\theta = \frac{dt}{2\sqrt{t}}$. Consequently, $I = 4\pi \left(\frac{a}{\pi}\right)^{3/2} \int\limits_{t=0}^{+\infty} e^{-at} t^2 \frac{dt}{2\sqrt{t}} = 2\pi \left(\frac{a}{\pi}\right)^{3/2} \int\limits_{t=0}^{+\infty} e^{-at} t^{3/2} dt$ and substituting the known definite integral $\int\limits_{x=0}^{+\infty} x^{3/2} e^{-ax} dt = \frac{3\sqrt{\pi}}{4a^{5/2}}$ [18], we get $I = 2\pi \left(\frac{a}{\pi}\right)^{3/2} \cdot \frac{3\sqrt{\pi}}{4a^{5/2}} = \frac{3kT}{m}$ and finally

$$< \rho_0 q_\omega(\underline{r'})\rho_0 q^*_\omega(\underline{r''}) >= \delta(\underline{r'} - \underline{r''}) \cdot C^2_{eff} \cdot \frac{3kT}{m}.$$

Returning to Equation (9), the wanted ensemble average of particle velocity becomes:

$$< u_\omega(\underline{r})u^*_\omega(\underline{r}) >= \frac{1}{\rho_0^2}\iiint\limits_V dr' \iiint\limits_V dr'' \cdot \left(\frac{\partial}{\partial r}G_\omega(\underline{r},\underline{r'})\right)$$

$$\cdot \left(\frac{\partial}{\partial r}G^*_\omega(\underline{r},\underline{r''})\right) \cdot \delta(\underline{r'}-\underline{r''}) \cdot C^2_{eff} \cdot \frac{3kT}{m} \Leftrightarrow$$

$$< u_\omega(\underline{r})u^*_\omega(\underline{r}) >= \frac{1}{\rho_0^2}\iiint\limits_V dr' \cdot \left(\frac{\partial}{\partial r}G_\omega(\underline{r},\underline{r'})\right) \cdot \left(\frac{\partial}{\partial r}G^*_\omega(\underline{r},\underline{r'})\right) \cdot C^2_{eff} \cdot \frac{3kT}{m} \Leftrightarrow$$

$$< u_\omega(\underline{r})u^*_\omega(\underline{r}) >= \iiint\limits_V C^2_{eff} \cdot \frac{3kT}{m\rho_0^2} dr' \left|\frac{\partial}{\partial r}G_\omega(\underline{r},\underline{r'})\right|^2 \overset{(10)}{\Leftrightarrow}$$

$$< u_\omega(\underline{r})u^*_\omega(\underline{r}) >= \iiint\limits_V \frac{3kT}{ml^2_{eff}} dr' \left|\frac{\partial}{\partial r}G_\omega(\underline{r},\underline{r'})\right|^2$$

In order to theoretically investigate, the difference in the estimated field between the normal state and the activation state, at the surface of the head model, the following Q ratio is estimated. Its numerator provides the difference of the field value generated at the activation and resting state, and its denominator the resting state field value per Kelvin degree. It must be noted here that U' is the value of the field that originates from both the internal source (IAS) and the head model (HMS), referring both to activation and resting state energy, while U is the value of the field originating only from the head model, referring to the resting state energy. As it is shown in the following equation, the two main reasons that cause the pressure field changes are the difference in the flow and consequently the local volume change between the two states, and the local temperature variations.

$$\frac{U'-U}{U} = \frac{\iiint\limits_{Vactiv} \frac{3k\delta T}{ml^2_{eff}} dr' \left|\frac{\partial}{\partial r}G_\omega(\underline{r},\underline{r'})\big|_{r=a}\right|^2}{\iiint\limits_{Vtot} \frac{3kT}{ml^2_{eff}} dr' \left|\frac{\partial}{\partial r}G_\omega(\underline{r},\underline{r'})\big|_{r=a}\right|^2} \Leftrightarrow$$

$$Q = \frac{\delta U}{U \cdot \delta T} = \frac{\iiint\limits_{Vactiv} dr' \left|\frac{\partial}{\partial r}G_\omega(\underline{r},\underline{r'})\big|_{r=a}\right|^2}{310(kelvin) \cdot \iiint\limits_{Vtot} dr' \left|\frac{\partial}{\partial r}G_\omega(\underline{r},\underline{r'})\big|_{r=a}\right|^2}$$

3. NUMERICAL RESULTS

The Q ratio as described above cannot be evaluated analytically but only with numerical methods. Therefore, MATLAB was used and R^3 space was approximated as a sum of finite volumes. For each finite volume in the position defined by $\underline{r'}$, the value of $\left|\frac{\partial}{\partial r}G_\omega(\underline{r},\underline{r'})\right|_{r=a}\Big|^2$ is calculated. Afterwards, a summation process takes place for the volumes of the internal sphere created by the point source and the sphere head model; hence the numerator and denominator of the Q expression are calculated:

$$Q = \frac{\delta U}{U \cdot \delta T} = \frac{\sum_{i=1}^{N_{ias}}\sum_{j=1}^{N_{ias}}\sum_{k=1}^{N_{ias}}\left|\frac{\partial}{\partial r}G_\omega(\underline{r},\underline{r'_{i,j,k}})\Big|_{r=a}\right|^2 (r'_i)^2\sin\theta'_j dr'_{ias}\,d\theta'_{ias}\,d\varphi'_{ias}}{310\cdot\sum_{i'=1}^{N_{hms}}\sum_{j'=1}^{N_{hms}}\sum_{k'=1}^{N_{hms}}\left|\frac{\partial}{\partial r}G_\omega\left(\underline{r},\underline{r'_{i',j',k'}}\right)\Big|_{r=a}\right|^2 (r'_{i'})^2\sin\theta'_{j'} dr'_{hms}\,d\theta'_{hms}\,d\varphi'_{hms}}$$

where

$$\left.\frac{\partial G_\omega(\underline{r},\underline{r'})}{\partial r}\right|_{r=a} = ik\sum_{l=0}^{\infty}\sum_{m=-l}^{l}\left(j_l(kr'_i)\left.\frac{\partial h_l^{(1)}(kr)}{\partial r}\right|_{r=a} - \frac{j_l(kr'_i)}{j_l(k\alpha)}h_l^{(1)}(k\alpha)\left.\frac{\partial j_l(kr)}{\partial r}\right|_{r=a}\right) Y_l^m(\theta,\phi)Y^{*m}_l(\theta'_j,\phi'_k)$$

for the internal activation sphere and

$$\left.\frac{\partial G_\omega(\underline{r},\underline{r'})}{\partial r}\right|_{r=a} = ik\sum_{l=0}^{\infty}\sum_{m=-l}^{l}\left(j_l(kr'_{i'})\left.\frac{\partial h_l^{(1)}(kr)}{\partial r}\right|_{r=a} - \frac{j_l(kr'_{i'})}{j_l(k\alpha)}h_l^{(1)}(k\alpha)\left.\frac{\partial j_l(kr)}{\partial r}\right|_{r=a}\right) Y_l^m(\theta,\phi)Y^{*m}_l(\theta'_{j'},\phi'_{k'})$$

for the head model sphere, assuming that each dimension of the R^3 space (r',θ',φ') is approximated by N_{ias} and N_{hms} finite points for the internal sphere and the head model respectively. In the above equations, (r'_i,θ'_j,ϕ'_k) represent the values of (r',θ',φ') at the (i,j,k)th point of the R^3 regarding the internal volume, and $(r'_{i'},\theta'_{j'},\phi'_{k'})$ represent the values of (r',θ',φ') at the (i',j',k')th point of the R^3 regarding the sphere head model, with the ranges of $(r',\theta',\varphi') \rightarrow (0-0.09\,m, 0-\pi, 0-2\pi)$. The radius of the head model sphere (HMS) is 9 cm, and the IAS has 1 cm radius. The average value of sound speed

Table 1. Q ratio for stable IAS position and different frequencies.

Position of IAS	5.4 cm from HMS
	$\theta = 0$
Frequency (Hz)	Q (1/Kelvin)
10	1.4688E-06
100	1.4684E-06
500	1.4830E-06
1000	1.5300E-06
5000	1.2912E-05
10000	2.1381E-04
15000	1.1540E-04
20000	4.5310E-04

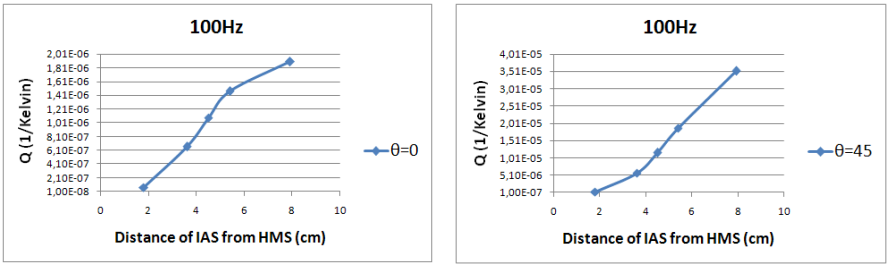

(a) (b)

Figure 2. Q ratio for different radial IAS positions at 100 Hz and (a) $\theta = 0°$, (b) $\theta = 45°$.

is 1500 m/s for the supposed medium, and the temperature of the head (model) takes the average value of 37°C or 310°K [19, 20].

The results of the computation are depicted in Table 1 and Figures 2, 3, 4, 5, 6 and 7 where the Q ratio values, from simulations of different positions of the IAS and different frequencies, are shown. More specifically in Table 1, Q values are presented for different frequencies and keeping the position of IAS stable, while in the following figures they are depicted in particular frequencies for different IAS positions (in radius and angle). The measurement point is always at $r = \alpha$ (the field is measured at the surface of the head model) and at angles $\theta = 0°$ and $\varphi = 0°$. All distances are measured from each sphere's center and all angles are calculated from the origin of the central coordinate system.

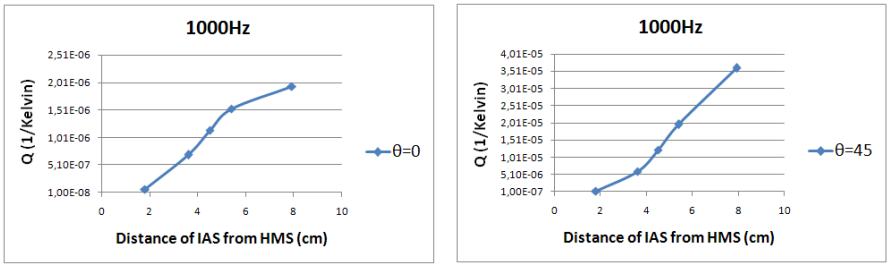

(a) (b)

Figure 3. Q ratio for different radial IAS positions at 1000 Hz and (a) $\theta = 0°$, (b) $\theta = 45°$.

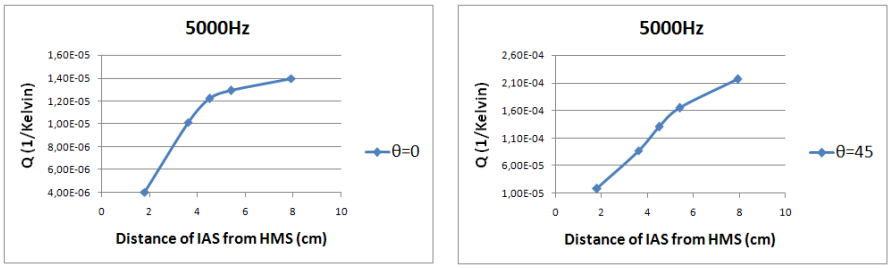

(a) (b)

Figure 4. Q ratio for different radial IAS positions at 5000 Hz and (a) $\theta = 0°$, (b) $\theta = 45°$.

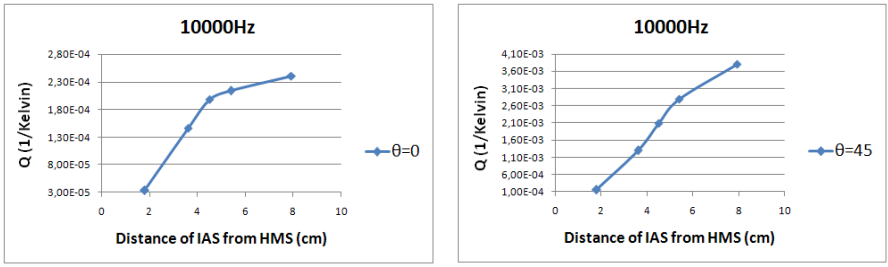

(a) (b)

Figure 5. Q ratio for different radial IAS positions at 10000 Hz and (a) $\theta = 0°$, (b) $\theta = 45°$.

Clear difference in the estimated field (particle velocity) between the resting state and the activation state can be observed in the figures above, a fact which, with the appropriate receiving system (PABMOS),

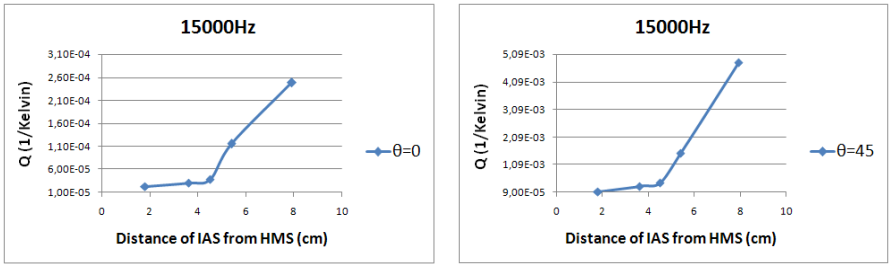

(a) (b)

Figure 6. Q ratio for different radial IAS positions at 15000 Hz and (a) $\theta = 0°$, (b) $\theta = 45°$.

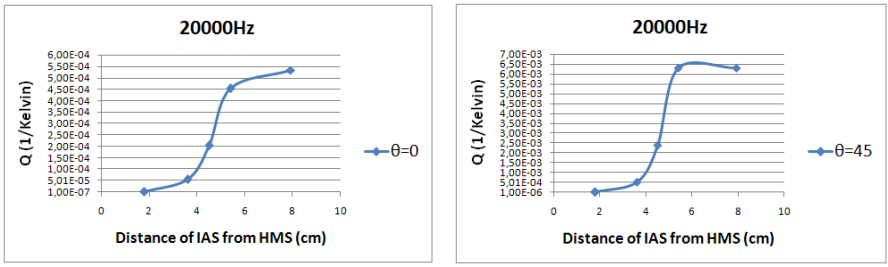

(a) (b)

Figure 7. Q ratio for different radial IAS positions at 20000 Hz and (a) $\theta = 0°$, (b) $\theta = 45°$.

can be utilized to distinguish normal state of the brain from activation ones originating from any abnormality or functional reason. This detection of the activation state is more evident at higher frequencies of the acoustic range (1 Hz–20 kHz) that is investigated in this research, as Q takes greater values there (Table 1 and Figs. 2–7).

Moreover, a very important feature of our research is evident from Figs. 2–7, where it can be seen that the radial alteration of Q ratio is as physiologically expected. Numerical results for IAS positions close to the HMS center and moving towards the HMS surface show that Q is significantly raised, resulting in better detection of an activation state that exists closer to head surface where a receiver sensor of the proposed system will be placed.

4. DISCUSSION AND CONCLUSIONS

In this paper, a semi-analytical technique has been presented for the study of the estimation of the pressure field at any spot of a

human head and especially at its surface, generated by an acoustic source inside it. A single layer Human Model Sphere is used as a human head while the internal source that simulates abnormalities or functional alterations in pressure field, is modeled with a smaller Activation Sphere. The proposed method is based on acoustics and its analogies to electromagnetism, with the use of Green's function. Several simulations have been performed to validate the method and obtain the necessary numerical results, at different frequencies and at several IAS positions. According to results, the detection of a pulsating acoustic source inside a head model is feasible at its surface with a better response at higher acoustic frequencies and for sources placed closer to the surface.

This research could be useful in practice and lead to the development of a receiving system which will be able to detect differences in pressure field (particle velocity particularly) that would arise from abnormalities or functional causes analyzed in the first section of this paper. Nevertheless, the practical value of such a system should be explored through the development of a prototype which will be used in phantom and later human experiments to initially assess proof of concept and following investigate its potential clinical perspective.

REFERENCES

1. Skudrzyk, E., *The Foundations of Acoustics*, Ch. 13, Springer-Verlag, Wien, New York, 1971.
2. Chaudhry, S. M. and A. M. Chaudhry, "System identification of acoustic characteristics of enclosures with resonant second order dynamics," *Progress In Electromagnetics Research*, Vol. 61, 89–110, 2006.
3. Bridger, K., "Brain assessment monitor," *J. Acoust. Soc. Am.*, Vol. 118, No. 4, 2114–2114, October 2005.
4. Karanasiou, I. S., N. K. Uzunoglu, and A. Garetsos, "Electromagnetic analysis of a non-invasive 3D passive microwave imaging system," *Progress In Electromagnetics Research*, Vol. 44, 287–308, 2004.
5. Karanasiou, I. S., N. K. Uzunoglu, and C. Papageorgiou, "Towards functional non-invasive imaging of excitable tissues inside the human body using focused microwave radiometry," *IEEE Trans. Microwave Theory and Tech.*, Vol. 52, 1898–1908, 2004.
6. Gouzouasis, I. A., K. T. Karathanasis, I. S. Karanasiou and N. K. Uzunoglu, "Contactless passive diagnosis for brain

intracranial applications: A study using dielectric matching materials," *Bioelectromagnetics*, (in press).

7. Karathanasis, K. T., I. A. Gouzouasis, I. S. Karanasiou, M. Giamalaki, G. Stratakos, and N. K. Uzunoglu, "Non-invasive focused monitoring and irradiation of head tissue phantoms at microwave frequencies," *IEEE Trans. Inf. Technol. Biomed.*, (in press).
8. Chen, G. P., W. B. Yu, Z. Q. Zhao, Z. P. Nie, and Q. H. Liu, "The prototype of microwave-induced thermo-acoustic tomography imaging by time reversal mirror," *Journal of Electromagnetic Waves and Applications*, Vol. 22, No. 11–12, 1565–1574, 2008.
9. Ismail, N. H. and A. T. Ibrahim, "Temperature distribution in the human brain during ultrasound hyperthermia," *Journal of Electromagnetic Waves and Applications*, Vol. 16, No. 6, 803–811, 2002.
10. Lazaro, A., D. Girbau, and R. Villarino, "Analysis of vital signs monitoring using an IR-UWB radar," *Progress In Electromagnetics Research*, Vol. 100, 265–284, 2010.
11. Ishimaru, A., *Electromagnetic Wave Propagation, Radiation, and Scattering*, Ch. 2, Prentice Hall Inc., New Jersey, 1991.
12. Lamb, H., *The Dynamical Theory of Sound*, 2nd Edition, Ch. 4, E. Arnold, 1910.
13. Morse, P. M. and H. Feshbach, *Methods of Theoretical Physics*, Part I, Ch. 7, McGraw-Hill, New York, 1953.
14. Morse, P. M. and H. Feshbach, *Methods of Theoretical Physics*, Part II, Ch. 13, McGraw-Hill, New York, 1953.
15. Rothwell Edward, J. and J. Cloud Michael, *Electromagnetics*, Appendix A, CRC Press, 2001.
16. Vanderlinde, J., *Classical Electromagnetic Theory*, 2nd edition, Ch. 10, Springer, 2004.
17. Lawrence, K. E., R. A. Frey, B. A. Coppens, and V. J. Sanders, *Fundamentals of Acoustics*, 3rd edition, Ch. 5, John Wiley & Sons, 1982.
18. Murray, R. S., *Schaum's Mathematical Handbook of Formulas and Tables*, 2nd edition, McGraw-Hill, 1999.
19. Gisolfi, V. C. and F. Mora, *The Hot Brain: Survival, Temperature and the Human Body*, The MIT Press, Cambridge, Massachusetts, 2000.
20. Elwassif, M. M., Q. Kong, M. Vazquez, and M. Bikson, "Bio-heat transfer model of deep brain stimulation-induced temperature changes," *Journal of Neural Engineering*, Vol. 3, 306–315, 2006.